IEEE Access
Multidisciplinary | Rapid Review | Open Access Journal

Received August 30, 2019, accepted September 6, 2019, date of publication September 10, 2019,
date of current version September 19, 2019.

Digital Object Identifier 10.1109/ACCESS.2019.2940499

Utilizing Anisotropic Fabrics Composites for High-Strength Soft Manipulator Integrating Soft Gripper

YINGLONG CHEN, (Member, IEEE), JUNHAO ZHANG, AND YONGJUN GONG
Naval Architecture and Ocean Engineering College, Dalian Maritime University, Dalian 116026, China

Corresponding author: Yongjun Gong (yongjungong@163.com)

This work was supported in part by the Fundamental Research Funds for the Central Universities under Grant 3132019351, and in part by the National Natural Science Foundation of China under Grant 51905067.

ABSTRACT Fabrics are promising materials to realize the high-strength soft robots as they are anisotropic, stretchable, and intrinsically high strength. Exploiting these properties, here we present the design and test of novel high-strength hydraulic soft manipulator modules composited different type of fabrics. The morphology of manipulator entirety is designed into an elephant's nose shape with three fabric-based soft actuators and a fiber-reinforced soft gripper with three fingers. The multi-degree of freedom of soft manipulator by filling different pressure into three actuators makes the gripper adaptable to gripping objects of various shapes, stiffness, and weights within a certain range. The soft manipulator modules are tested to characterize its workspace, torque output, and rotational stiffness. Gripping function tests are also conducted to estimate the achieved degree of functions of the gripper. Functional tests verify that the proposed soft manipulator and gripper has achieved expectations, so, it has great potential applications in production and daily life.

INDEX TERMS High-strength soft manipulator, anisotropic fabrics, soft arm, gripper.

I. INTRODUCTION

Soft actuators are increasingly attracting the interest of researchers in recent years. Compared with conventional rigid actuators, soft actuators are safer and more adaptable, which can interact friendly with humans and interact with unstructured environment better [1]. According to previous research, soft actuators mainly include fluid-driven soft actuators [2]–[4], shape memory alloy (SMA)-driven actuators [5], [6], shape memory polymer (SMP)-driven actuators [7], [8], particle jamming [9], [10], dielectric elastomer [11], [12]. A common feature of these actuators is that they depend on elastomeric materials for the body, such as silica gel and urethane. These soft materials have many advantages, including the ability to co-mold multiple other materials, chemical and heat resistance, and the ability to withstand large deformations while conducting complex ranges of motion (ROM).

The associate editor coordinating the review of this manuscript and approving it for publication was Yingxiang Liu.

However, properties such as stiffness and strength of material make elastomeric materials not ideal for many applications such as flexible seal and grabbing operation, because they are often prone to tears, punctures, and tensile failures when strained. For the soft robotics, low strength results in low driving force, soft manipulator or gripper cannot support or grab high-weight objects. Fiber-reinforced actuators can greatly increase the strength of actuators made of soft materials [2], but with the increase of driving pressure, the expansion between fibers is unavoidable, and even the fibers will cut off the soft actuator when the actuator is pressurized to a certain extent. Fabrics are promising materials, because they have high strength and inherent anisotropy [13], [14]. Fabric-based actuators increase driving pressure by adding a fabric layer (common woven fabric) outside the actuator [15], [16], they have advantages of high flexibility and relative high force output [3], [29], [30] but the fabric will restrict ROM of soft actuator due to poor stretchability.

Pneumatically actuated method is most classical among soft actuators [17], which have been applied to soft robots

and bionics very commonly. However, insufficient strength of soft actuators remains a serious problem, pneumatic system has some limitations because gases have compressibility and there is a certain risk of high pressure, such as explosion. In the previous research, the test pressure is mostly below 0.3 MPa [3], [22], [23]. In contrast, hydraulically actuated soft actuators have better strength and stiffness than pneumatic ones [18]–[21]. Therefore, it is necessary to study a hydraulically driven soft manipulator and gripper with novel materials to improve the strength and stiffness without changing compliance.

Here, we present the design and test of a novel high-strength and high-stiffness hydraulic soft manipulator composited with anisotropic fabrics that can support and grab objects of different sizes, shapes, stiffness and weights. Our design includes fabric investigation and selection, structure of soft manipulator and structure of soft gripper. Testing is conducted to contain: ①fabric characteristics. ②pressure-displacement characteristics, end force output and dynamic response of actuators of soft manipulator. ③workspace, torque output and rotational stiffness of soft manipulator modules. ④tip force output, bending angle and stiffness of actuators of soft gripper. Our highlight is to exploit the anisotropy of the fabrics to increase the driving pressure and ROM of the soft actuator greatly. We added the driving pressure to 1.5MPa, and the soft actuator has no signs of leakage or blasting, so the strength and stiffness of the soft actuator are improved significantly, which has been demonstrated in this paper.

Main contributions of this work include: ①We investigated two novel types of fabrics (knitted fabric and elastic fabric), which can perform greater anisotropy than traditional woven fabric. We developed the high-strength soft manipulator modules exploiting the anisotropy of the fabrics, which can produce high strength, large ROM, and high stiffness.

II. DESIGN

A. FABRIC INVESTIGATION AND SELECTION

Based on the requirement of high strength and large ROM, the two modules of soft manipulator and gripper we designed (see Fig. 1) need to have different functions. This section mainly introduced the fabrics selection of different modules. For Module 1, it should have certain stiffness and rigidity, which is antagonistic to the driving water pressure. So, Module 1 needs a textile which possess high strength, high modulus and stretches ability in one direction and stretches performance poorly in the perpendicular direction. Knitted fabric can exhibit anisotropic behavior because their looped construction creates inherent structural deformation. Knitted materials can exhibit more obvious anisotropic behavior because their looped construction will produce inherent structural deformation. Knitted fabrics are suitable for applications requiring anisotropy because their structures are relatively rigid in one direction and compliant in the other. In addition, knitted fabrics are usually balanced

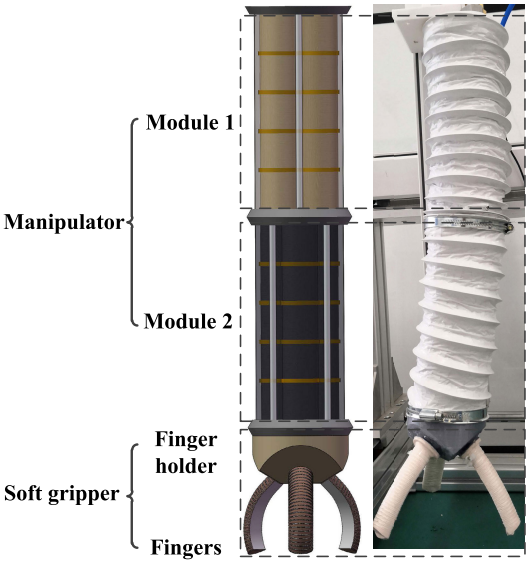

FIGURE 1. The combination of high-strength soft manipulator and soft gripper. The manipulator consists of two modules with different functions, and the gripper consists of a finger holder and three fingers. The left picture is the model and the right one is entity.

fabrics, which means that their looped construction has front-back and left-right symmetry, respectively. [24] The material chosen for the knitted fabric is nonnegligible factor, the tensile properties and fracture strength of nylon, aramid and polyethylene textiles were tested and the result is that aramid textiles have the best properties. We chose a commercially knitted aramid fabric (Aramid 1414), and we cut 15 sections of samples with length of 200 mm and width of 30 mm, the results of the universal tension machine (FL-8613, see Fig. 4c) test (warp and weft direction) are shown in Fig. 2a.

For Module 2, under the condition of high stiffness of Module 1, it is necessary to achieve more ROM, which requires that the actuators can be significantly elongated in the axial direction when pressurized, simultaneously, it is necessary to restrict the radial expansion, which is the useless work of water pressure. Therefore, the fabric chosen in Module 2 needs more significant anisotropy than in Module 1. Elastic fabric (the warp yarns are made of latex, and the weft yarns are polyester low-elastic yarns), is particularly suited for the Module 2 because its structure is relatively stiff in one direction and compliant significantly in the other. We chose a plain elastic fabric (latex and polyester), for its low weight, sewability properties and brilliant anisotropy, and the test result shows in Fig. 2b (warp and weft direction).

The physical properties of elastic fabrics are like a light spring, which can produce huge deformation in one direction and hardly deformation in the other. The mechanical response of the elastic fabric (warp direction) can be nicely expressed by Hooke's law: $x_F = F_{st}/\ k_{el}$, where $\boldsymbol{F_{st}}$ is the pulling force on elastic fabrics, $\boldsymbol{k_{el}}$ is the modulus of elasticity and $\boldsymbol{x_F}$ is a deformable quantity. Finally, we use a sewing machine (FHSM-201) to sew elastic fabrics into cylinders along the warp direction.

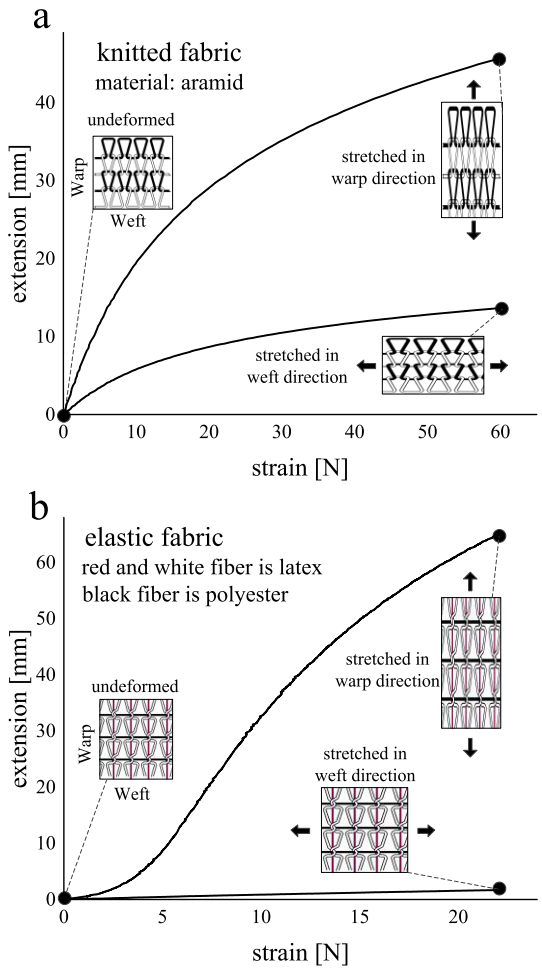

FIGURE 2. Testing fabric mechanical anisotropy for high-strength actuators. Load-strain characteristics of aramid knitted fabric(a) and elastic fabric(b).

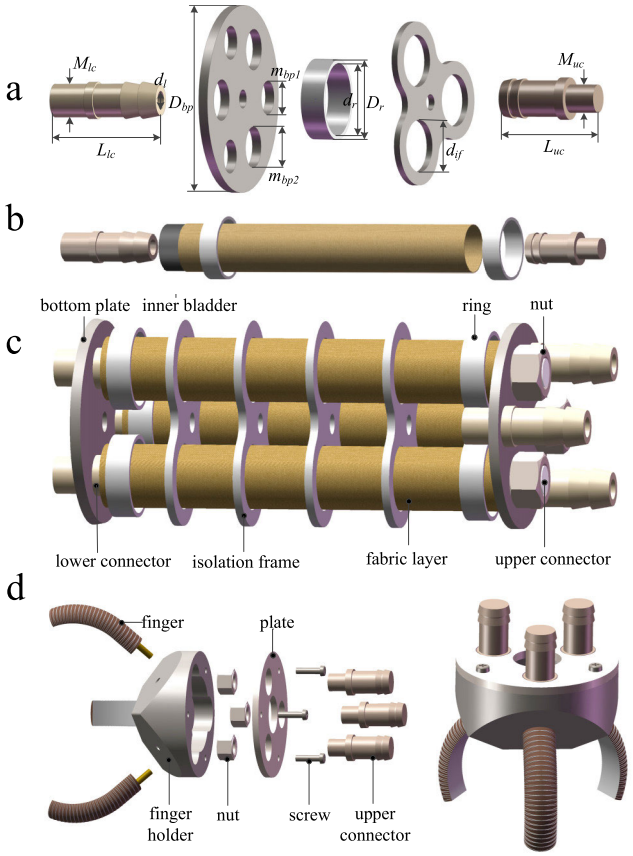

FIGURE 3. (a) The shape and dimensions of the main parts of the soft manipulator module. (b) Exploded view of the actuator assembly. (c) The detailed structure of the soft manipulator module. (d) Structure and exploded view of the soft gripper.

B. STRUCTURE OF SOFT MANIPULATOR

The proposed soft manipulator is designed to support and grab high-weight or fragile objects by combining soft gripper. Simultaneously, soft arm needs to be highly flexible, which requires modules to be able to extend and bend by pressurizing different actuators with different hydraulic pressure, which makes the soft manipulator much easier to adapt surroundings.

Fig. 3b shows assembly of one actuator of one module of soft manipulator and Fig. 3c shows one module of soft manipulator, which is mainly composed of three actuators, and the three actuators are installed on the bottom plate (can be understood as the joint of the arm.) by threaded connection, respectively, and the upper connectors and nuts connection are used to clamp the bottom plate of the next module to achieve modularization. The function of the isolation frames is to reduce the coupling between the actuators when the manipulator is bent.

The actuator consists of external fabric layer (knitted fabric or elastic fabric) and inner bladder, which is made of silica gel (ELASTOSIL® M 4601). The bladders were constructed in a multistep process. ELASTOSIL® M 4601, divided into A and B groups, the mixing ratio is 20:1. Component B contains platinum catalyst to improve the solidification rate of component A. Mixed silica gel was put into a centrifugal mixer (MWZ-2, 220v/50Hz, 6Kw) for full mixing, and then put into the vacuum generator (2XZ-2, pump speed 2L/s,) to remove bubbles. The 3D printing mould (CR −10S Pro 3D Printer) is sealed with tape (PTFE), then the silica gel is poured into the mould. After baking and solidification (vacuum dryer, DZF-6053), the bladder is prepared (characteristics: the density is 1.01 g / mm^2, the tensile strength is 5 N/ mm^2, the elongation at break is 700 %, and the tear strength is greater than 30 N/ mm, linear shrinkage rate is less than 1%). Finally, the bladder was inserted into the fabric shell, and the open edge of the fabric cylinder was hand sewn to avoid any possible damage of the bladder. The upper and lower ends of fabric and bladder are fixed with pipe press (YS-20Z) by upper connectors (blocking flow), lower connectors (through flow) and rings. The material of connectors and rings is aluminum alloy, which makes the actuators have light weight and sealing performance. Therefore, the actuators we designed mainly include two types: Aramid Fabric Actuator (AFA) and Elastic Fabric Actuator (EFA), and the manipulator modules mainly include

TABLE 1. geometric parameters of the soft manipulator module.

Parameter	*Symbol*	*Values*
External threads of lower connector	M_{lc}	M18×1.5 mm
Effective length of lower connector	L_{lc}	60 mm
Flow diameter of lower connector	d_l	10 mm
Number of bottom plate	s	3
Diameter of bottom plate	D_{bp}	100 mm
Matching thread between bottom plate and lower connector	m_{bp1}	M18×1.5 mm
Matching diameter between bottom plate and upper connector	m_{bp2}	φ 22 mm
Inner diameter of ring	d_r	34 mm
outer diameter of ring	D_r	38 mm
Inner diameter of isolation frame	d_{if}	32 mm
External threads of upper connector	M_{uc}	M14×1.5 mm
Effective length of upper connector	L_{uc}	50 mm
Thickness of actuator	B	4 mm
Length of an actuator	L	185 mm
Weight of one module of the manipulator	G	608 g

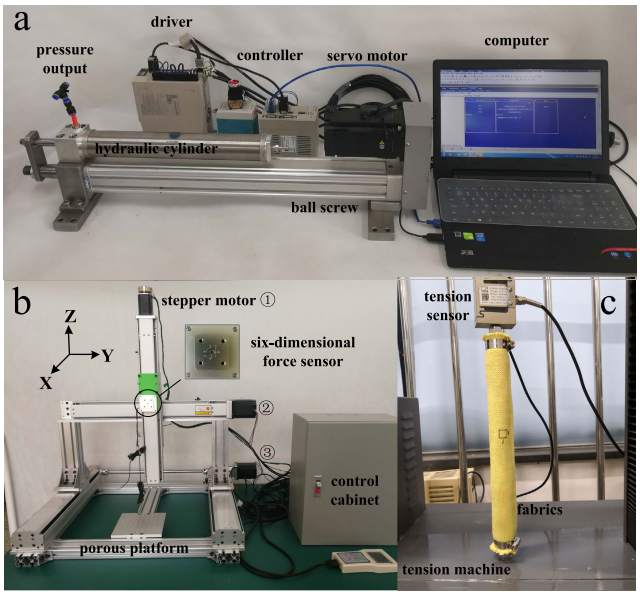

FIGURE 4. (a) Experiment setup for testing. (b) Water hydraulic direct drive system. (c) fabrics tension test.

two types: Aramid Fabric Manipulator (AFM) and Elastic Fabric Manipulator (EFM).

Geometric parameters of the proposed soft manipulator are shown in Fig. 3a and listed in Table 1. These parameters are mainly designed according to the required strength and high-driving force. For example, if the thickness of the actuator is too thick, it will reduce the ROM and if it is too thin, it will cause insufficient strength. Therefore, we tested many times and analyzed the results to get the most suitable size. In order to reduce the coupling between the actuators, the distance of the threaded holes on the bottom plate, that is, the position of the three actuators, should be as small as possible but not too large. In addition to the high-driving force and ROM, dynamic response of manipulator is also considerable, which means the initial volume of actuator should be small. So, the length, diameter and number of actuators are all relevant to the dynamic response.

C. STRUCTURE OF SOFT GRIPPER

Fig. 3d shows assembly and structure of soft gripper. The connection method between the gripper and the manipulator is that the three upper connectors of the manipulator are connected with nuts, in order to clamp the upper plate, then connects the finger holder (manufactured by 3D printer) with screws. The material of the finger is also silicone, and the manufacturing process is the same as that of the manipulator. We wrapped polyethylene fibers around soft fingers to increase finger strength and limit the radial expansion of the fingers. We used glass fibers as limiting layer (not elongated) on the inner side of the fingers, so that the finger will bend to one side when pressurized. The connection between finger and water pipe (rigid, external thread M5) is connected and sealed with cable tie and glue and the three fingers are connected to the finger holder by threads. The method to control the gripper is that one water pipe drives three fingers, that is, after pressurization, three fingers bend at the same time.

III. TEST

This section mainly includes the test of the actuators (AFA and EFA) of the manipulator (pressure-displacement characteristics, end force output and dynamic response) and the test of manipulator modules (workspace, output torque and rotational stiffness), including AFM and EFM. We also tested tip force, bend angle and stiffness of actuator of soft gripper. Fig. 4 shows the setup used in the test, mainly including the water hydraulic direct drive system (Fig. 4a) and the three-degree-of-freedom test platform (Fig. 4b). Hydraulic direct drive system is mainly composed of servo motor (Sgm7fj-08A7C6E, Japan), ball screw and hydraulic cylinder (Bimba, H-3112-DBA, America). It can provide a maximum water pressure of about 1.5 MPa. The control signal is transmitted from PC to servo motor, then the rotary motion is changed into linear motion through ball screw, and then the extension and retraction of piston rod in hydraulic cylinder are controlled to generate driving water pressure.

The three-degree-of-freedom test platform we used mainly consists of three stepping motors (86BYGH126, China), four sliding module frames and a control cabinet. The X-axis is designed by connecting a pair of parallel modules with square sheet metal. Y and Z axes module body cross installation is assembled on X axes module sliding platform by gantry form through bracket square sheet metal. OY axis and OZ axis are driven by stepping motor to realize the movement

of Y axis and Z axis; OX axis is driven by stepping motor, and two module slides are driven by screw to realize the movement of X axis. A porous test platform is installed at the bottom center of the three-degree-of-freedom test platform to locate and install the actuators, manipulator and gripper.

A. TEST OF THE SINGLE ACTUATOR

1) PRESSURE-DISPLACEMENT CHARACTERISTICS

Pressure-displacement characteristics of the actuator were tested: the residual air in the internal actuator and the entire drive system pipeline is drained before the test starts, so that the pipeline is completely filled with water. We fixed the actuator on the porous platform, controlled the driving water pressure, and recorded the length and diameter of the actuator when the water pressure was 0.1 MPa, 0.2 MPa ...1 MPa, respectively, and the water pressure was measured using a pressure transmitter (TY-811, −0.1MPa∼32MPa). The purpose of measuring the length is to characterize the end displacement of the actuator by the change of the length. The larger the end displacement, the larger the bending angle of the manipulator and the larger the motion space. The purpose of testing the diameter of the actuator is to verify that the fabric layer whether play a limiting role and how much useless work is done by water pressure. We have done 15 tests on AFA and EFA respectively. The experimental results are shown in Fig. 5.

In the process of increasing water pressure, the length of AFA extends from 185 mm to 213 mm, the elongation rate is 14.6% (blue curve), the diameter increases by 0.8 mm (red curve), that is, the AFA expands by 0.8 mm. The length of EFA extends from 185 mm to 303 mm, the elongation is 63.8%, and the diameter increases by 0.5 mm. This meets our anticipated design requirements. When the actuator is being pressuring, it will produce F_a (thrust force produced by water pressure acting on the top of the actuator) and F_b (resistance to the elongation of the actuator, mainly caused by fabric and bladder). The elongation process of AFA can be divided into two stages. 0∼0.5 MPa is a fast elongation stage, in which F_a is greater than F_b because of the fabric is slack at this time , the actuator elongates rapidly. 0.5 MPa∼1 MPa is a slow elongation stage, the resistance of aramid knitted fabric is particularly high, the thrust force increases faster so that the length increases slower, in which F_a is similar to F_b and the fabric is now under tension. For EFA, because of the structure of elastic fabric, the elastic fabric is always subjected to stress by the latex in the warp direction during the elongation process, and the latex has good tensile properties, so the elongation and pressure of EFA have a certain linear relationship.

2) OUTPUT FORCE

End output force of the actuators were tested: we tested the output force of the actuator at different end positions. For example, for AFA, we controlled the water pressure to be maintained at 0 MPa, 0.1 MPa, 0.2 MPa, 0.3 MPa, 0.5 MPa,

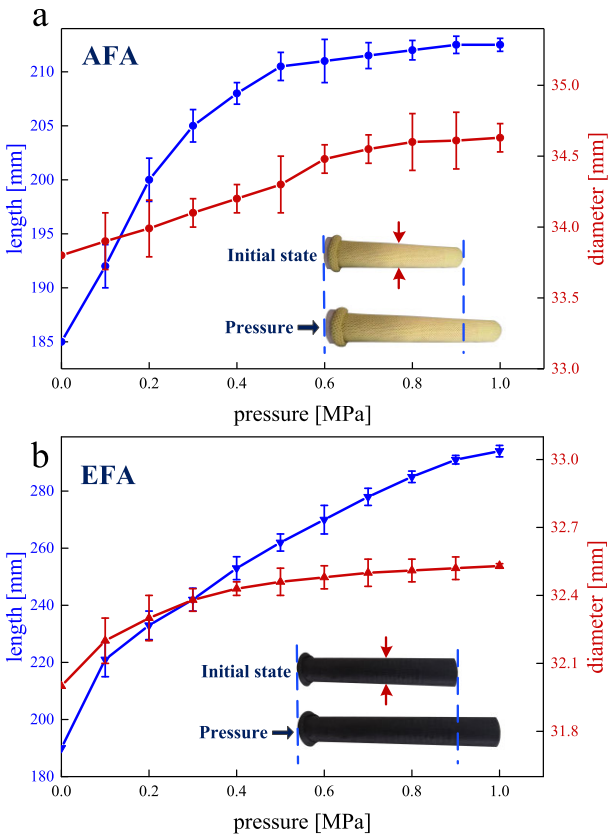

FIGURE 5. Experimental results of the pressure-displacement characteristics of AFA(a) and EFA(b). The blue line is the length of the actuator when it is pressurized, and the red line is the diameter of the actuator.

and the corresponding end displacements are $L_0 = 0$ mm, $L_1 = 7$ mm, $L_2 = 15$ mm, $L_3 = 20$ mm, and $L_4 = 25$ mm, respectively. At this time, the OZ axis was adjusted so that a six-dimensional force sensor (NC-6DT80, Germany) is in critical contact with the end of actuator, and the driving pressure is increased to record the relationship between the force and pressure in Fig. 6.

The relationship between output force and pressure is approximately positive, which shows that the fabric layer plays a significant role in limiting expansion. Water pressure almost all acts on the bottom of the actuator, making the actuator elongate. But why not be completely positive correlation is because we have done several sets of experiments, the repetition rate is not excellent. In fact, it reveals some common challenges faced by soft robots, that are poor nonlinearity and repeatability, which are the main factors affecting accuracy. Nonlinearity mainly depends on the non-linear mechanics of soft materials, such as superelasticity of silica gel and fabrics. Moreover, the soft actuator of manipulator has a cylinder shape, which makes it tend to perform lateral bending slightly, thus, adds to irregularity of the end force if any nonsymmetricity of geometry is induced in fabrication.

3) DYNAMIC RESPONSE

Dynamic characteristics is an important factor affecting the performance of the actuator. Therefore, we tested the

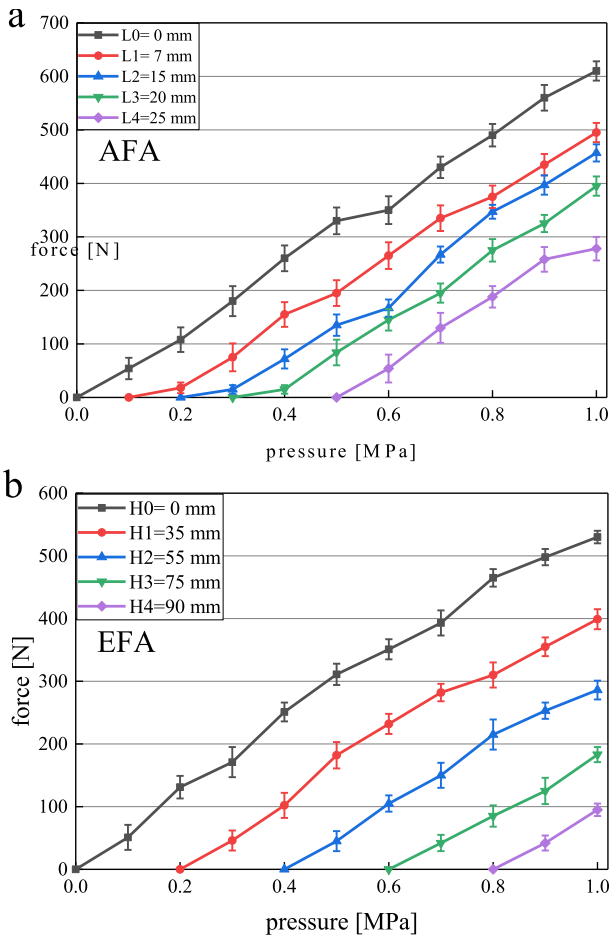

FIGURE 6. Experimental results of the end force output of AFA(a) and EFA(b).

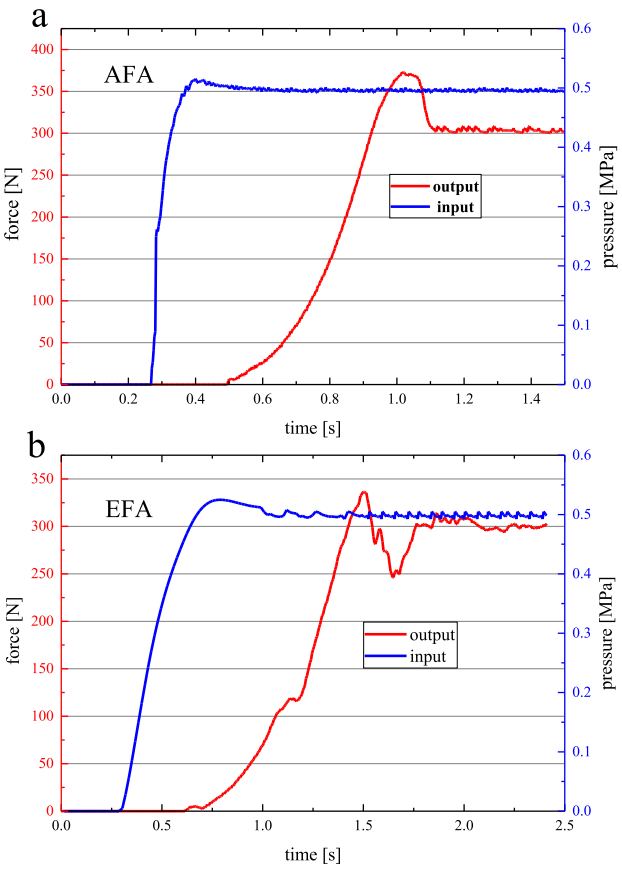

FIGURE 7. Experimental results of the dynamic response of AFA(A) and EFA(b), the blue line is the input pressure and the red line is the output force of the actuator, respectively.

relationship between the output force of the actuator and time. Because the response time mainly depends on the pressure and flow rate entering the actuator, the internal volume of the actuator and the length and diameter of the pipeline. The speed of the servo motor is set to 2000 r/min, the length of the pipe is 132 mm and the diameter is 6 mm. The pipe and the actuator were filled with water ahead of time.

AFA reaches a stable output force at 1.08 s and EFA at 1.77 s (see Fig. 7). There is no doubt that as a result of these hardware facilities, we can increase the pressure and flow rate by increasing the motor speed and replacing large diameter and small length water pipes, thereby improving the response time. We will do specific research on manipulator control in the future. In addition, the actuator itself has a certain overshoot and hysteresis, because AFA starts with signal output at 0.49 s and EFA starts at 0.56 s.

In order to investigate the overshoot and hysteresis of the soft actuator, the relationship between input pressure and time was recorded. It can be found that there is a slight overshoot before the input pressure reaches stable 0.5 MPa, which is the main reason for the overshoot of the output force. When there is pressure input, the force is not immediately output, which is due to the resistance of the bladder and fabric. The hysteresis is mainly caused by two factors. The first is due to the relative friction between the inner bladder and the outer fabric layer, thus consuming part of the driving force, which is called rate-independent hysteresis, which cannot be avoided by slowing the actuation speed [25]. The second one is the rate-dependent hysteresis, which is induced by the lag between input and output [26]. For example, elongating of the soft actuator may lag behind varying of the driving pressure or sensing of the sensor may lag behind elongation of the soft actuator, which can be reduced by slowing the actuation speed. After several tests, we find that the rate-dependent hysteresis can be almost eliminated if the driving pressure is below 0.2 MPa/s. Therefore, for reducing the hysteresis, dynamic response experiments are all conducted below 0.2 MPa/s.

Although the proposed soft actuator responds to force similar to the previous one [22] that has a response time of 1.33 s, the output force of the proposed actuator is 302N, and the previous one is 34 N.

B. TEST OF MANIPULATOR MODULES

In this section, the tests of manipulator modules (AFM and EFM) mainly includes workspace, torque and rotational stiffness. Firstly, we defined the parameters of the

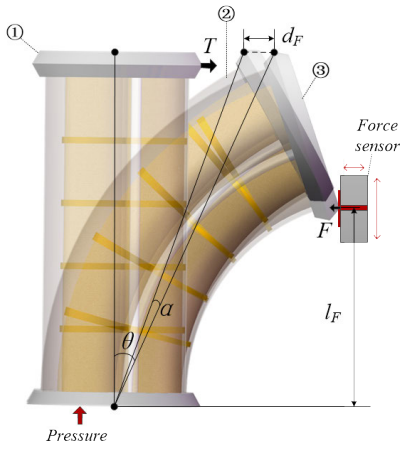

FIGURE 8. Parameters to define the motion of manipulator module. *F* is an external force applied by the six-dimensional force sensor and under the action of *F*, the manipulator module generates rotational angle α and displacement d_F.l_F is the force arm of *F*. θ is the bend angle of the module and *T* is the torque generated by the module when pressured. ① ② ③ represent the different postures of the manipulator module respectively, ① is the natural posture when the module is not pressurized. ① → ③ is the process of bending when a certain pressure is applied. This process produces the bend angle θ. ③ → ② is a process in which the posture of the module changes when the force F is applied by the sensor. This process produces the rotational angle α.

manipulator modules (see Fig. 8) in order to explain the performance of the arm more clearly.

1) WORKSPACE

Workspace of modules includes bend angle and elongation length. Bend angle (θ in Fig. 8) is an important feature of the modules' workspace, which determines the maximum flexibility of manipulator. Since modules are composed of three actuators, its bend angle is symmetrical. When one or two actuators are pressurized, the module will bend. When three actuators are simultaneously filled with the same pressure, the module will stretch. For example, Fig. 9a is the experimental result of EFM and it contains the following information: ①the degree of bending of the module when two actuators are pressurized, and the black dot represents the position at which the end of the module can reach. ②the elongation of the three actuators when they are simultaneously filled with pressure. We tested the bend angle (AFM and EFM) of the modules in the plane, as shown in Fig. 9b.

As we predicted, the bending angle of EFM is larger than that of AFM under the same driving pressure. This is because the elongation of elastic fabric is superior than that of aramid fabric, which is also consistent with the pressure-displacement characteristics of the actuator tested before. The bending angle of the AFM is 72° under the water pressure is 1 MPa, there is no obvious change in the bending angle with the pressure continues to increase, but the stiffness at this time is large significantly, and the human hand cannot change its posture.

To measure achievable motion space of the overall manipulator integrating gripper, we installed the manipulator on

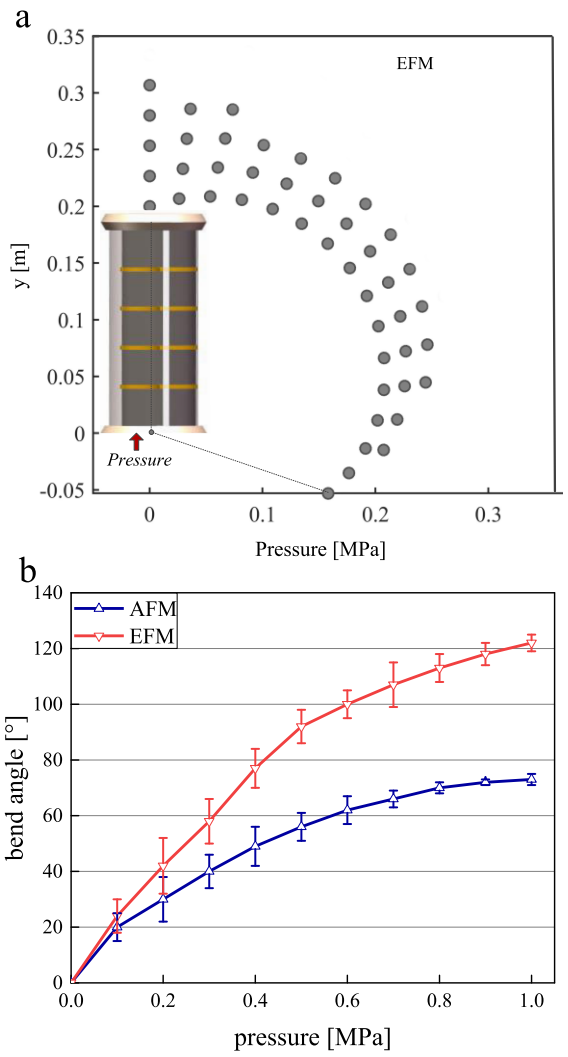

FIGURE 9. Workspace of the manipulator modules. (a) workspace of EFM and the "●" indicates any point in the workspace and the workspace contains so many such points that single "●". (b) Experimental results of the bend angle of AFM (blue line) and EFM (red line).

the test platform. Then, the actuators of manipulator were pressurized from natural state (Fig. 10a) to partial flexion (in the plane) (Fig. 10f), and to full flexion (Fig. 10b, d). Because of its own weight, the overall bend angle of the manipulator is different from that of the module bending test. The soft manipulator can also achieve out-of-plane bending by applying different pressures in different actuators. (Fig. 10c, e)

2) TORQUE OUTPUT

When the manipulator module bends, it generates torque (***T*** in Fig. 8) in the direction of bending. The output torque largely determines how much weight the manipulator can support. We tested the output torque of the manipulator module at different postures. We used 3D printing technology to make the corresponding fixture to make the end of the manipulator module fully contact with the sensor. By adjusting the driving hydraulic pressure, the manipulator module

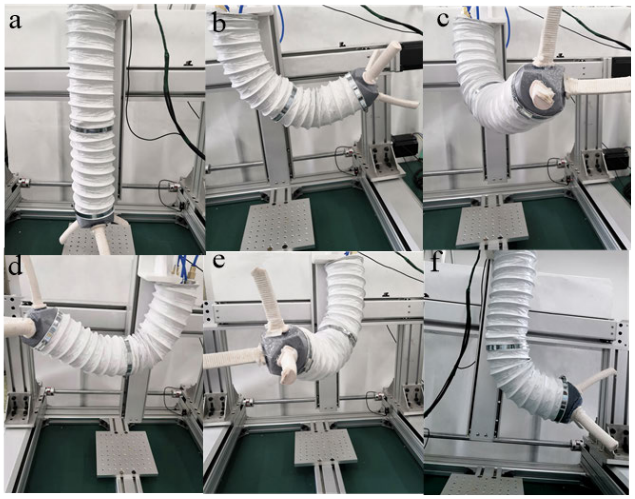

FIGURE 10. Achievable motion space of the manipulator. (a) natural state. (b) full bend to the right in the plane. (c) full bend to the right outside the plane. (d) full bend to the left in the plane. (b) full bend to the right outside the plane. (b) partial bend to the right in the plane.

bends and maintains this posture, for example, for the AFM, we controlled the driving water pressure to be 0, 0.1 MPa, 0.2 MPa, 0.3 MPa, 0.4 MPa, 0.6 MPa and 0.8 MPa. At this time, the corresponding bending angles are 0°, 19°, 32°, 45°, 52°, 61° and 70°. At this time, we increased the hydraulic pressure and collected the output torque of the manipulator module, which is accomplished by the six-dimensional force sensor. The experimental results are shown in Fig. 11.

Compared with EFM, the output torque of AFM has a good linear relationship with driving pressure, and generates more torque, with a measured maximum of 11.2 Nm at 0° of bending when pressured at 1 MPa. In comparison, the EFM generates 6.4 Nm under the same bending and pressure conditions. Because the AFM and EFM use different fabric materials and structures in their construction, the better linearity and torque achieved at any given pressure with the AFM relative to the EFM one can be attributed entirely to the deformation in the textile.

As to why the output torque of EFM is non-linear, it can be seen from *II. – A. FABRIC INVESTIGATION and SELECTION* that there are tension differences in the fabric layer, which results in different stiffness of the two manipulator modules. The AFM can keep constant curvature bending during the applying pressure, while EFM shows larger and irregular curvature after 0.5 MPa and this leads to a smaller output torque. This problem just reflects the current research hotspot of soft manipulator, that is, the difficulty of establishing variable curvature model.

3) ROTATIONAL STIFFNESS

When it comes to supporting objects, the rotational stiffness k_{sup} [27] is an important factor. In this section, the rotational stiffness of manipulator modules is defined as

$$k_{\text{sup}} = {F \cdot l_F}/{\alpha} \tag{1}$$

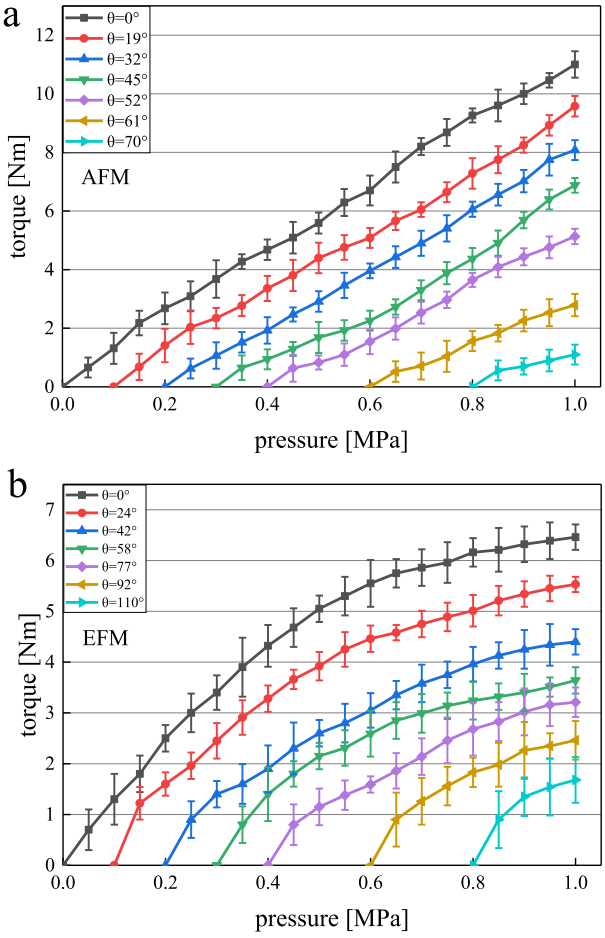

FIGURE 11. Experimental results of the torque output of AFM(a) and EFM(b).

where F is applied by six-dimensional force sensor and α is the rotational angle. Theoretically, α is calculated based on the displacement of the module's endpoint $\boldsymbol{d_F}$, the length of force arm $\boldsymbol{l_F}$. For experimental test, it can be directly measured.

We fixed the manipulator module on the experimental platform. Two actuators of module are filled with pressure to make it bend and another actuator is filled with appropriate pressure to keep the manipulator module in this posture. At this time, adjusted the six-dimensional force sensor on Z axis to make the center point of the sensor touch the endpoint of the manipulator module (Fig. 12a). The sensor is then controlled to drive the manipulator module to rotate (d_F = 3 mm, see Fig. 8), which can be accurately accomplished by the control handle. Then the rotation angle a of the arm module in the process of driving is calculated, and the rotational stiffness can be calculated. The experimental results are shown in Fig. 12c.

Stiffness of the proposed soft manipulator can be tuned by varying charging water pressure, which makes it possible to support objects of different weight. Compared with EFM, AFM has greater stiffness, which is due to the inherent pressure-displacement characteristics and output force of

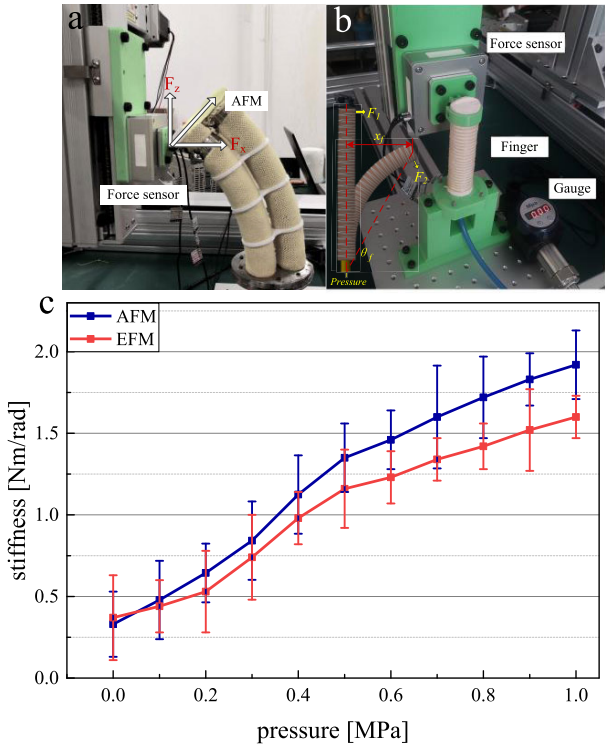

FIGURE 12. (a) Rotational stiffness the manipulator modules. Experiment method for testing. (b) Parameters to define the motion of soft finger. F_1 and F_2 are the tip force of finger under different pressures, respectively. θ_f is the bend angle of the soft finger. x_f is the tip displacement of the soft finger. Experiment setup for testing tip force and stiffness. (c) Experimental results of the stiffness of AFM (blue line) and EFM (red line).

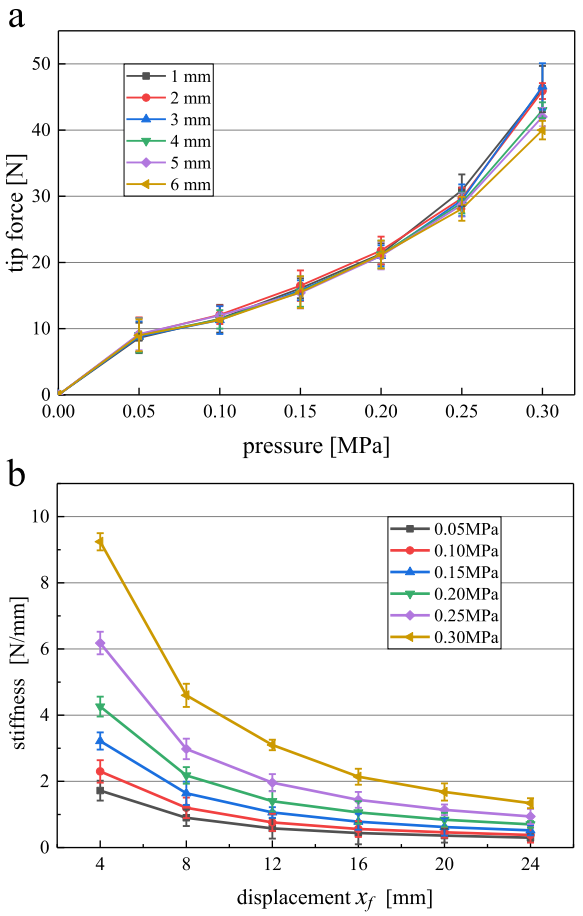

FIGURE 13. (a) Experimental results of the tip force of soft finger in different pressure. (b) Experimental results of the stiffness of soft finger in different displacements.

AFA and EFA, but this meets our expectations. Compared with the previous soft manipulator module [18] that can tune stiffness in 0.3–7.2 N/cm, our proposed soft manipulator module has a larger stiffness.

C. TEST OF GRIPPER

Soft actuators of gripper are mainly characterized by tip force and stiffness. In order to test the tip force of the soft finger more accurately (F_i in the Fig. 12b), we used 3D printer to make a fixture matching the finger, which shown in Fig. 12b, and we tested the tip force of the soft finger at different displacements. The experimental results are shown in Fig. 13a and it shows that the tip force increases exponentially with the increase of driving pressure. When the displacement $x_f = 6$ mm and the water pressure rises from 0.05 MPa to 0.15 MPa, the tip force of soft finger changes from 8N to 16N, and when the water pressure rises from 0.15 MPa to 0.3 MPa, the tip force of soft finger changes from 16N to 42N, which is related to the speed of bend angle of the soft finger when it is pressurized [28].

The stiffness of the soft finger determines how much weight it can grasp. If the stiffness is insufficient, it cannot grasp the heavy object. We defined the stiffness model of the soft finger as follows: $k_{gra} = F_i/x_f$, where $\boldsymbol{F_i}$ is tip force of soft finger in pressure, and $\boldsymbol{x_f}$ is the corresponding displacement. $\boldsymbol{k_{gra}}$ is stiffness of soft finger.

Before the start of the experiment, adjusted the three-degree-of-freedom test platform to keep the end of the soft finger in contact with the six-dimensional force sensor. Then, the pressure is filled into the inner chamber of the finger, and the port and the driving pipe at the bottom of the finger are cut off by the ball valve (Q11F, China) to keep the pressure in the inner chamber of the finger. Under the same tip force of the soft finger, the displacements of the six-dimensional force sensors at the end of the soft finger are 4 mm, 8 mm, 12 mm, 16 mm, 20 mm and 24 mm, respectively. During the change of displacement, the soft finger will automatically produce the same displacement with the six-dimensional force sensor because of its internal pressure, and the soft finger will bend. The stiffness changes of the soft finger under different displacements were measured. To ensure the accuracy of the test results, six groups of driving pressures were selected, which are 0.05 MPa, 0.1 MPa, 0.15 MPa, 0.2 MPa, 0.25 MPa and 0.3 MPa, respectively.

When the displacement is 4 to 8 mm, the stiffness of the soft finger changes the most (Fig. 13b), the resistance to overcome the elongation of the finger is the smallest. When the driving pressure of the finger inner chamber is constant, the stiffness decreases gradually with the finger

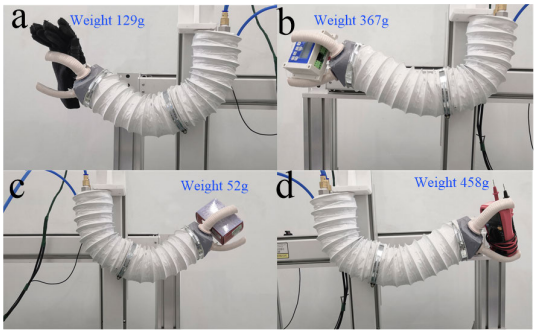

FIGURE 14. The experiment of gripping multiple kinds of objects: (a) gloves, (b) panel, (c) boxes, (d) avometer.

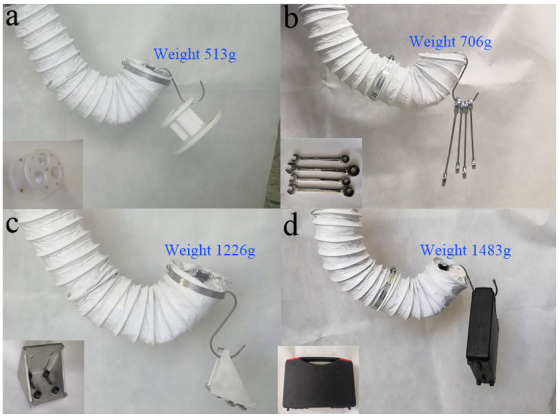

FIGURE 15. The experiment of supporting relative heavy objects: (a) 3D-printed part, (b) wrenches, (c) angle iron, and (d) toolbox.

displacement increasing slowly from 4mm to 20mm, and tends to soften. This is because under the same initial driving pressure, the larger the displacement, the larger the deformation of the finger, and the greater the internal pressure drop. In addition, the distance between the twin helix is enlarged due to expansion, and the thickness of the elongation surface of the finger decreases, resulting in the weakening of the stiffness of the soft finger.

IV. FUNCTION

To demonstrate the ability of soft manipulator integrating gripper to grip multiple objects, we carried out function experiments. The gripping ability for multiple kinds of objects is an important indication to evaluate the performance of the soft manipulator, and the test results are shown in Fig. 14. It can grip objects that have different shapes and stiffnesses, and experiments showed that it can grip gloves, control panel, boxes, and avometer (Fig. 14a–d).

During the experiment, the manipulator and gripper can easily support and grab objects with a weight of < 500 g. Next, we tested the load capacity of the manipulator, and the manipulator can easily support a 3D-printed part by hanging an S-hook (weight 513g, Fig. 15a). Also, the manipulator can support 706g of four different types of wrenches relatively easily, and there is a little deformation in its axial direction (Fig. 15b). And an angle iron of 1226g can be supported by the soft manipulator (Fig. 15c). Further, a toolbox of 1483g is selected as a cantilever object, although the manipulator produces a certain axial deformation, it can still carry the weights, and the deformation can be recovered automatically after the weights are removed. (Fig. 15d). (Supplementary Video S1). When supporting relatively heavy objects, Module 2 tends to become thicker. The reason is that in order to improve the stiffness of the arm, we reduce the number of isolation frames and the inner side actuator of the bending manipulator is filled with negative pressure.

V. CONCLUSION AND FUTURE WORK

Exploiting the anisotropic, stretchable, and intrinsically high strength properties of fabrics, we present the design and test of novel high-strength hydraulic soft manipulator modules composited different type of fabrics. The morphology of manipulator entirety is designed into an elephant's nose shape with three fabric-based soft actuators and a fiber-reinforced soft gripper with three fingers. The multi-degree of freedom of soft manipulator by filling different pressure into three actuators makes the gripper adaptable to gripping objects of various shapes, stiffness, and weights within a certain range. The soft manipulator modules are tested to characterize its workspace, torque output, and rotational stiffness. Functional tests verify that the proposed soft manipulator and gripper has achieved expectations, so, it has great potential applications in production and daily life.

Tests of manipulator actuators (AFA and EFA) show that AFA can elongate from 0 to 28 mm with an initial value of 185 mm, simultaneously, expand 0.8 mm, produce maximum output force of 608 N, response to force with time of 1.08 s, with experimental maximum pressure of 1 MPa. EFA can elongate from 0 to 118 mm with an initial value of 185 mm, simultaneously, expand 0.5 mm, produce maximum output force of 534 N, response to force with time of 1.77 s. The manipulator modules(AFM and EFM) show that AFM can perform maximum bend angle is 72°, produce maximum of 11.2 Nm at 0° of bending when pressured, and produce maximum rotational stiffness is 1.9 Nm/rad at 1 MPa. EFM can perform maximum bend angle is 121°, produce maximum of 6.4 Nm at 0° bending, and produce maximum rotational stiffness is 1.6 Nm/rad, respectively.

Tests of soft gripper show that when the displacement of finger is 6 mm and the water pressure rise from 0.05 MPa to 0.3 MPa, the tip force of soft finger changes from 8 N to 42 N. In addition, under constant pressure, the stiffness decreases with increasing displacement.

In functional tests, the proposed gripper is verified to be adaptable to gripping objects of different shapes, sizes, weights and the high strength and stiffness of soft manipulator are fully exposed. It has potential applications in production and daily life.

Future research will focus on modeling of the soft manipulator and its force and motion control methods. The stress-strain relationship of tensile tests of the fabric materials can be applied to construct a quasi-static or dynamic analytical

model to predict output force and motion of the actuator in different working conditions.

ACKNOWLEDGMENT

The authors thank the reviewers for their elaborate and incisive suggestions.

REFERENCES

[1] P. Polygerinos, N. Correll, S. A. Morin, B. Mosadegh, C. D. Onal, K. Petersen, M. Cianchetti, M. T. Tolley, and R. F. Shepherd, "Soft robotics: Review of fluid-driven intrinsically soft devices; Manufacturing, sensing, control, and applications in human-robot interaction," *Adv. Eng. Mater.*, vol. 19, no. 12, 2017, Art. no. e201700016.
[2] J. Bishop-Moser and S. Kota, "Design and modeling of generalized fiber-reinforced pneumatic soft actuators," *IEEE Trans. Robot.*, vol. 31, no. 3, pp. 536–545, Jun. 2015.
[3] L. Cappello, K. C. Galloway, S. Sanan, D. A. Wagner, R. Granberry, S. Engelhardt, F. L. Haufe, J. D. Peisner, and C. J. Walsh, "Exploiting textile mechanical anisotropy for fabric-based pneumatic actuators," *Soft Robot.*, vol. 5, no. 5, pp. 1–13, 2018.
[4] X. Liang, H. Cheong, Y. Sun, J. Guo, C. K. Chui, and C.-H. Yeow, "Design, characterization, and implementation of a two-DOF fabric-based soft robotic arm," *IEEE Robot. Autom. Lett.*, vol. 3, no. 3, pp. 2702–2709, Jul. 2018.
[5] L. Peng and G. Song, "An innovative ultra-capacitor driven shape memory alloy actuator with an embedded control system," *Smart Mater. Struct.*, vol. 23, no. 8, 2014, Art. no. 085013.
[6] C. H. Pan and Y. B. Wang, "Development of a novel micro-actuator driven by shape memory alloy," *Solid State Phenomena*, vol. 164, pp. 9–14, Jun. 2010.
[7] J. Leng, L. Xin, Y. Liu, and S. Du, "Shape-memory polymers and their composites: Stimulus methods and applications," *Prog. Mater. Sci.*, vol. 56, no. 7, pp. 1077–1135, 2011.
[8] Y. Yang, Y. Chen, W. Ying, and Y. Li, "3D printing of shape memory polymer for functional part fabrication," *Int. J. Adv. Manuf. Technol.*, vol. 84, nos. 9–12, pp. 2079–2095, 2016.
[9] W. Ying, Y. Chen, Y. Yang, and Y. Li, "A soft robotic spine with tunable stiffness based on integrated ball joint and particle jamming," *Mechatronics*, vol. 33, pp. 84–92, Feb. 2016.
[10] M. V. Hecke, "Jamming of soft particles: Geometry, mechanics, scaling and isostaticity," *J. Phys., Condens. Matter*, vol. 22, no. 3, 2009, Art. no. 033101.
[11] H. Godaba, J. Li, Y. Wang, and J. Zhu, "A soft jellyfish robot driven by a dielectric elastomer actuator," *IEEE Robot. Autom. Lett.*, vol. 1, no. 2, pp. 624–631, Jul. 2016.
[12] M. Haruna, K. Kubo, K. Fukusumi, and T. Tamida, "Development of soft actuator: Mechanism with vibration element using dielectric elastomer to generate large displacement," *Proc. SPIE*, vol. 6524, Apr. 2007, Art. no. 652418.
[13] W.-L. Wu, H. Hamada, and Z. Maekawa, "Computer simulation of the deformation of weft-knitted fabrics for composite materials," *J. Textile Inst.*, vol. 85, no. 2, pp. 198–214, 1994.
[14] X. Gu, H. Jing, and M. Huang, "Anisotropy of elasticity and fabric of granular soils," *Granular Matter*, vol. 19, no. 2, p. 33, 2017.
[15] Y. Wang, C. Gregory, and M. A. Minor, "Improving mechanical properties of molded silicone rubber for soft robotics through fabric compositing," *Soft Robot.*, vol. 5, no. 3, pp. 272–290, 2018.
[16] H. K. Yap, P. M. Khin, T. H. Koh, Y. Sun, X. Liang, J. H. Lim, and C.-H. Yeow, "A fully fabric-based bidirectional soft robotic glove for assistance and rehabilitation of hand impaired patients," *IEEE Robot. Autom. Lett.*, vol. 2, no. 3, pp. 1383–1390, Jul. 2017.
[17] T. Takizawa, T. Kanno, R. Miyazaki, K. Tadano, and K. Kawashima, "Grasping force estimation in robotic forceps using a soft pneumatic actuator with a built-in sensor," *Sens. Actuators A, Phys.*, vol. 271, pp. 124–130, Mar. 2018.
[18] P. Polygerinos, Z. Wang, K. C. Galloway, R. J. Wood, and C. J. Walsh, "Soft robotic glove for combined assistance and at-home rehabilitation," *Robot. Auto. Syst.*, vol. 73, pp. 135–143, Nov. 2015.
[19] Y. Nishioka, M. Uesu, H. Tsuboi, and S. Kawamura, "Proposal of an extremely lightweight soft actuator using plastic films with a pleated structure," in *Proc. 19th Int. Conf. Mechtron. Mach. Vis. Pract.*, Auckland, New Zealand, 2013, pp. 474–479.
[20] E. Acome, S. K. Mitchell, T. G. Morrissey, M. B. Emmett, C. Benjamin, M. King, M. Radakovitz, and C. Keplinger, "Hydraulically amplified self-healing electrostatic actuators with muscle-like performance," *Science*, vol. 359, no. 6371, pp. 61–65, 2018.
[21] D. F. Walczyk and Y.-T. Im, "A Hydraulically-Actuated Reconfigurable Tool for Flexible Fabrication: Implementation and Control," *J. Manuf. Sci. Eng.*, vol. 122, no. 3, pp. 562–568, 2000.
[22] Y. Fei, J. Wang, and W. Pang, "A novel fabric-based versatile and stiffness-tunable soft gripper integrating soft pneumatic fingers and wrist," *Soft Robot.*, vol. 6, no. 1, pp. 1–20, 2018.
[23] J. Yi, X. Chen, C. Song, and Z. Wang, "Fiber-reinforced origamic robotic actuator," *Soft Robot.*, vol. 5, no. 1, p. 81, 2017.
[24] S. C. Ray, *Fundamentals and Advances in Knitting Technology*. New Delhi, India: Woodhead Publishing India, 2012.
[25] B. D. Coleman and M. L. Hodgdon, "A constitutive relation for rate-independent hysteresis in ferromagnetically soft materials," *Int. J. Eng. Sci.*, vol. 24, no. 6, pp. 897–919, 1986.
[26] V. Hassani, T. Tjahjowidodo, and T. N. Do, "A survey on hysteresis modeling, identification and control," *Mech. Syst. Signal Process.*, vol. 49, nos. 1–2, pp. 209–233, 2014.
[27] Y. Li, Y. Chen, Y. Yang, and W. Ying, "Passive particle jamming and its stiffening of soft robotic grippers," *IEEE Trans. Robot.*, vol. 33, no. 2, pp. 446–455, Apr. 2017.
[28] S. Arimoto, K. Tahara, M. Yamaguchi, P. T. A. Nguyen, and M.-Y. Han, "Principles of superposition for controlling pinch motions by means of robot fingers with soft tips," *Robotica*, vol. 19, no. 1, pp. 21–28, 2016.
[29] J. H. Low, W. W. Lee, P. M. Khin, N. V. Thakor, S. L. Kukreja, H. L. Ren, and C. H. Yeow, "Hybrid tele-manipulation system using a sensorized 3-D-printed soft robotic gripper and a soft fabric-based haptic glove," *IEEE Robot. Autom. Lett.*, vol. 2, no. 2, pp. 880–887, Apr. 2017.
[30] R. Q. van der Linde, "Design, analysis, and control of a low power joint for walking robots, by phasic activation of McKibben muscles," *IEEE Trans. Robot. Autom.*, vol. 15, no. 4, pp. 599–604, Aug. 1999.

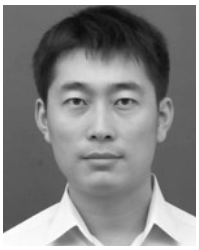

YINGLONG CHEN received the B.Eng. and Ph.D. degrees in mechatronic control engineering from Zhejiang University, Zhejiang, China, in 2008 and 2013, respectively. From 2013 to 2016, he has been a Research Assistant with the School of Mechanical Engineering, Zhejiang University. Since 2017, he has been an Assistant Professor with the Naval Architecture and Ocean Engineering, Dalian Maritime University. His research interests include fluid power transmission and control, the advanced motion control of mechatronic systems, and robotics.

JUNHAO ZHANG received the B.Eng. degree in mechanical and electronic engineering from the Liaoning University of Technology, Jinzhou, China, in 2018. He is currently pursuing the master's degree with the Naval Architecture and Ocean Engineering College, Dalian Maritime University. His research interests include soft robotics, and fluid power transmission and control.

YONGJUN GONG received the Ph.D. degree in mechatronic control engineering from Zhejiang University, Zhejiang, China, in 2005. Since 2005, he has been a Professor with the Naval Architecture and Ocean Engineering College, Dalian Maritime University. His research interests include fluid power transmission and control, water hydraulics, and underwater tools systems.